

One step to synthesize the nanocomposites of graphene nanosheets and N-doped titania nanoplates with exposed {001} facets for enhanced visible-light photocatalytic activity

Jian-Wen Shi · Chang Liu · Hui-Ying Ai ·
Jian-Wei Chen · Chong Xie · Guodong Li ·
Shenghui Yang · Shi Li

Received: 24 December 2014 / Accepted: 21 April 2015 / Published online: 20 May 2015
© Springer Science+Business Media Dordrecht 2015

Abstract Due to large particle size, low specific surface area, and the high recombination rate of the photo-generated electron–hole pairs, micrometer-sized N-doped TiO₂ plates (NTP) with {001} facets generally present lower visible-light photocatalytic activity. In order to solve these problems, the nanocomposite photocatalysts consisted of graphene nanosheets (GR) and N-doped TiO₂ nanoplates (NTNP) with exposed {001} facets were synthesized by a sol–gel process for the first time. The physical and chemical properties of the resultant nanocomposites

(NTNP/GR) were studied in detail, and their photocatalytic activities were investigated by the photocatalytic decoloration of methylene blue solution under visible-light irradiation ($\lambda > 420$ nm). Owing to smaller particle size (about 25 nm) and higher specific surface area in comparison with micrometer-sized NTP, the photocatalytic activity of NTNP was improved effectively. Due to the effective charge anti-recombination of graphene, the photocatalytic activity of nanocomposite NTNP/GR was further improved. Due to the competition for light absorption between graphene and NTNP, there was an optimal ratio (1.0 %, the weight percentage of graphene to TiO₂) between graphene and NTNP for the maximum of visible-light photocatalytic activity.

J.-W. Shi (✉) · C. Liu · C. Xie · S. Yang
Center of Nanomaterials for Renewable Energy, State Key Laboratory of Electrical Insulation and Power Equipment, School of Electrical Engineering, Xi'an Jiaotong University, Xi'an, People's Republic of China
e-mail: jianwen.shi@mail.xjtu.edu.cn; shijwn@163.com

H.-Y. Ai · J.-W. Chen
Key Laboratory of Urban Pollutant Conversion, Institute of Urban Environment, Chinese Academy of Sciences, Xiamen 361021, Fujian, People's Republic of China

G. Li
State Key Laboratory of Inorganic Synthesis and Preparative Chemistry, College of Chemistry, Jilin University, Changchun 130012, People's Republic of China

S. Li
Department of Environmental Science and Engineering, China University of Petroleum, Qingdao 266580, People's Republic of China

Keywords Photocatalysis · TiO₂ · Graphene · Nanocomposite · Visible light

Introduction

Controllable growth of metal oxides or semiconductors with high reactive facets has aroused great interest in the recent years owing to their superior intrinsic shape-independent properties in large numbers of applications, such as photocatalysis (Grabowska et al. 2014), photoelectrocatalysis (Zhang et al. 2011), hydrogen production (Li et al. 2013), solar cell (Sun et al. 2014), and lithium ion battery (Chen et al. 2010). As a dominant semiconductor photocatalyst, anatase

TiO₂ crystals with high reactive {001} facets have been investigated since the pioneering work (Yang et al. 2008), and many research results have proved that the photocatalytic activity of anatase TiO₂ crystals could be enhanced significantly owing to the exposure of high reactive {001} facets (Yang et al. 2009b; Han et al. 2009; Zhang et al. 2009; Liu et al. 2010b). However, the photocatalytic activity of anatase TiO₂ with high reactive {001} facets is still limited by narrow light absorption (only UV with wavelength below 387 nm can be used) (Hoffmann et al. 1995; Diebold 2003; Fujishima et al. 2008; Jing et al. 2013). For utilizing solar light, visible-light responsive TiO₂ crystals with exposed {001} facets are highly desired.

On the other hand, ion doping, especially nonmetal doping has been considered as an effective means to promote the visible-light response of TiO₂ (Chen and Mao 2007; Yu et al. 2009). For example, Asahi et al. found that N-doped TiO₂ displayed visible-light photocatalytic activity (wavelength, 500 nm) for the photocatalytic degradation of methylene blue (Asahi et al. 2001). Khan et al. found that C-doped TiO₂ could respond visible light with wavelength of 535 nm (Khan et al. 2002). Therefore, incorporating dopants into anatase TiO₂ crystals with exposed {001} facets may be a promising attempt to explore new photocatalysts with high activity under visible-light irradiation. In this regard, a series of progress has been made, and nonmetal-doped TiO₂ plates (e.g., N, S, C) with exposed {001} facets have been successfully prepared (Liu et al. 2009, 2010a; Yu et al. 2010), and their photocatalytic activities under visible light have been confirmed. However, these nonmetal-doped TiO₂ plates with exposed {001} facets are micrometer in size, which inevitably results in its low specific surface areas, and then hampers the improvement of photocatalytic ability. In our previous work (Shi et al. 2014a), we prepared micrometer-sized N-doped TiO₂ plates (NTP) with exposed {001} facets, and demonstrated that the obtained NTP presented photocatalytic active for methylene blue (MB) decomposition under visible light. Unfortunately, their visible-light photocatalytic activity was low; only about 55 % MB was decomposed after 120 min reaction owing to large particle size (2.5 μm), low specific surface area (1.76 m² g⁻¹), and the high recombination rate of the photo-excited electrons and holes. Nanoparticles have smaller particle size and larger specific surface area in comparison with micrometer-sized particles.

Smaller particle size is helpful to the transfer photo-excited carriers to the surface of photocatalyst, and larger specific surface area is advantageous to pre-adsorption of reactants on the surface of photocatalyst. Both of them are helpful to restrain the recombination of photo-excited electrons and holes. Therefore, it can be deduced that nanometer-sized nonmetal-doped TiO₂ plates with exposed {001} facets may be a promising approach to develop new photocatalysts with higher visible-light activity. In our recent work (Ai et al. 2014), we successfully prepared N-doped TiO₂ nanoplates (NTNP) with exposed {001} facets by a sol-gel method. Compared with micrometer-sized N-doped TiO₂ plates, the visible-light photocatalytic activity of NTNP was impressively improved; more than 90 % MB was removed after 120 min visible-light irradiation ($\lambda > 420$ nm). However, there is still room for further enhancement in the visible-light photocatalytic activity of NTNP if suitable measures are taken to more effectively inhibit the recombination of photo-excited electrons and holes.

Due to excellent mobility of charge carriers (200,000 cm² V⁻¹ s⁻¹), large specific surface area (calculated value ~ 2630 m² g⁻¹), and good mechanical stability (Lee et al. 2008; Allen et al. 2010), graphene (GR) has attracted great interest in the recent years. Considering its excellent mobility of charge carriers, graphene could be a superior candidate to combine with TiO₂ for the effective charge anti-recombination. Up to now, a large number of publications have reported that the recombination of photo-generated electron-hole pairs can be effectively restrained due to the fact that graphene acts the transporter of electrons in TiO₂/GR composites (Xiang et al. 2012; Zhang et al. 2012). In our previous work (Shi et al. 2014b), we synthesized the composite photocatalysts consisted of graphene nanosheets and micrometer-sized N-doped TiO₂ plates with exposed {001} facets by a one-pot hydrothermal process, and we found that graphene nanosheets acted as transporter of photo-excited electrons to prevent the recombination of photo-generated electrons and holes, which significantly improved the visible-light photocatalytic activity of the composite photocatalysts.

Based on these previous results (Ai et al. 2014; Shi et al. 2014a, b), in present work, we explored a path to further improve the visible-light photocatalytic activity of TiO₂ by incorporating graphene nanosheets and NTNP with exposed {001} facets to synthesize

nanocomposite photocatalysts. The structural properties of the prepared samples were characterized by XRD, TEM, XPS, DRS, and BET, and their photocatalytic performances were tested by the photocatalytic decoloration of MB under visible-light irradiation. As expected, the visible-light photocatalytic activity of nanocomposite photocatalysts NTNP/GR was significantly enhanced. To our knowledge, this is the first time to synthesize the nanocomposite photocatalysts consisted of NTNP with exposed {001} facets and graphene nanosheets.

Experimental

Synthesis of NTNP

NTNP with exposed {001} facets were synthesized by a sol–gel method. First, 6.85 ml of tetrabutyl titanate was dispersed in 15.5 ml of absolute ethanol under vigorous stirring for 30 min in a conical flask with cover (solution A). Second, 0.37 g of NH_4F , 7.75 ml of absolute ethanol, 8 ml of acetic acid, and 2.88 ml of pure water were mixed in a beaker (solution B). Then, solution B was dropwise added into solution A with vigorous magnetic agitation. Subsequently, the obtained mixture (sol) was kept in incubator chamber at 90 °C for 12 h to get gel. Then, the obtained gel was dried at 80 °C in an oven, porphyzied into powders, and then calcined at 500 °C in air for 2 h, resulting NTNP sample.

Synthesis of NTNP/GR composites

Graphene oxide (GO) was synthesized by the modified Hummers' method, and the detailed process can be found in our previous publication (Shi et al. 2014b). Similar to the synthesis of NTNP, NTNP/GR composites were synthesized by one step sol–gel method. In a typical synthesis route, a given amount of GO powder was added into solution A under vigorous agitation to form well-distributed solution. Then, solution B was added into solution A drop-by-drop under vigorous stirring. Subsequently, the obtained mixture was kept in incubator chamber at 90 °C for 12 h to get gel. Then, the obtained gel was dried at 80 °C in an oven. Subsequently, the dry gel was porphyzied into powders, and then was calcined at 500 °C in nitrogen atmosphere for 2 h. In the process

of heat-treatment, GO was reduced into GR, resulting in NTNP/GR sample. In order to investigate the effect of graphene content on the photocatalytic activity of NTNP/GR composites, the percentages of graphene to TiO_2 were designed as 0.5, 1.0, 1.5, and 2 % by adjusting the added weight of GO powder, and the resulting samples were marked as NTNP/GR- x , where $x = 0.5, 1.0, 1.5, \text{ and } 2.0$, respectively.

Characterization

X-ray diffraction (XRD) was carried out at room temperature with an X' pert PROMPD diffractometer (PANalytical, Holland) with copper $\text{K}_{\alpha 1}$ radiation. Transmission electron microscope (TEM) was performed on JEM 2100 (JEOL, Japan). X-ray photoelectron spectroscopy (XPS) was done on an ESCALAB250 (Thermo Scientific, USA) with aluminum K_{α} radiation. UV–vis diffuse reflectance spectra were recorded with a UV-2450 spectrophotometer (Shimadzu, Japan) equipped with an integrating sphere, and the baseline correction was verified by using a calibrated barium sulfate. The nitrogen adsorption was performed at 77 K by using an ASAP 2010 analyzer (Micromeritics, USA), and the Barrett–Joyner–Halenda (BJH) pore diameter distribution curves were obtained from the desorption branch and specific surface areas were obtained according to the Brunauer–Emmett–Teller (BET) model. Photoluminescence (PL) spectra were recorded at room temperature by using a fluorescence spectrophotometer (Hitachi, F-4600) with an excitation wavelength of 300 nm.

Experimental procedures of photocatalytic decoloration

The photocatalytic experiment was carried out in a photo reaction system [as illustrated in our previous publication (Shi et al. 2012c)], and MB was used as a model pollutant. Visible-light was provided by a 1000 W Xe lamp (the UV irradiation below 420 nm wavelength was cut-off by a glass filter). The Xe lamp was placed in the center of a water-cooled quartz jacket. At the side of quartz jacket with a distance of 40 mm, a cylindrical vessel with a volume of 50 ml was utilized as the reactive bottle to load reaction solution. In the bottom of the reactive bottle, a magnetic stirrer was equipped to realize efficient

dispersion. At every experiment, 50 mg of photocatalyst was added into 50 ml of MB solution with the concentration of 10 mg l^{-1} to form suspension under stirring. After achieving adsorption equilibrium, Xe lamp was turned on to irradiate the suspension. During the whole experiment, the suspension was agitated continuously. At given interval, 3 ml of suspension was taken out and immediately centrifuged to eliminate the solid particles. The absorbance of the filtrate was measured by a spectrophotometer at the maximum absorbance peak of MB (665 nm).

Results and discussion

Crystal phase

The results of XRD test of all samples including NTNP and NTNP/GR are displayed in Fig. 1. The peaks at $2\theta = 25.28^\circ$, 37.80° , 48.05° , 53.89° , 55.06° , and 62.69° (JCPDS: 00-021-1272), which can be assigned to (101), (004), (200), (105), (211), and (204) planes of anatase TiO_2 , respectively, appear in all XRD patterns, indicating that anatase TiO_2 has formed in all samples. The characteristic peak of GO at $2\theta = 9.8^\circ$ [as shown in Fig. 2 in our previous publication (Shi et al. 2014b)] cannot be observed in the XRD patterns of all NTNP/GR samples, implying that GO has been reduced into GR in the process of

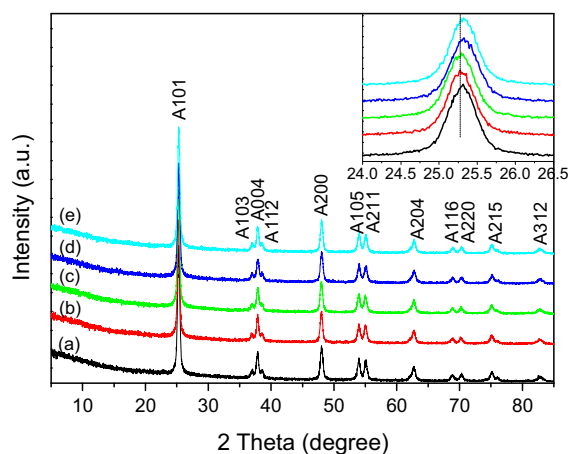


Fig. 1 The XRD patterns of samples (A anatase): *a* NTNP, *b* NTNP/GR-0.5, *c* NTNP/GR-1.0, *d* NTNP/GR-1.5, *e* NTNP/GR-2.0. (Color figure online)

heat-treatment. Furthermore, there are no typical diffraction peaks of the separate graphene in the XRD patterns of all NTNP/GR samples, which can be ascribed to the facts that both the amount of graphene in samples and the diffraction intensity of graphene are relatively low (Zhang et al. 2010a). However, by careful comparing, a slight shift of the diffraction peak at $2\theta = 25.28^\circ$ to higher angle with the increase of GR in the composite can be detected (as shown in the inset in Fig. 1), which can be ascribed to the fact that the main peak of graphene at 26.1° has been shielded by the main peak of anatase TiO_2 at 25.28° (Xu et al. 2010; Zhang et al. 2010b).

Morphology

Figure 2 shows the TEM images of typical sample NTNP/GR-1.0 with different magnifications. A large number of particles are anchored on a large piece of satin-like GO nanosheet (Fig. 2a). These particles are well faceted nanocrystals with uniform particle size (Fig. 2b, the partial enlarged image from the region marked with white square in Fig. 2a), and the square, hexagon, and rhombus shapes can be found by viewing from different directions (as marked in Fig. 2b), which are owing to highly truncated octahedral structure, implying that titania nanoplates with exposed {001} facets have formed. As shown in the inset in Fig. 2b, these nanoplates present a square outline, and the two square surfaces are {001} facets and the eight isosceles trapezoidal surfaces are {101} facets of anatase TiO_2 crystal (Yang et al. 2008). The side length of TiO_2 plates is approximately 25 nm and the percentage of {001} facets is about 40 %. The HR-TEM of one typical plate (the inset in Fig. 2a) clearly shows the continuous atomic planes with a spacing of 0.20 nm, which is corresponding to the {200} planes of anatase TiO_2 crystals, demonstrating that the two square surfaces are {001} facets.

Surface element composition

Figure 3a shows the XPS full survey spectrum of typical sample NTNP/GR-1.0. These elements of Ti, O, N, C, and F have been detected. The peak of F1s can be ascribed to the grafted F ions (Liu et al. 2009; Shi et al. 2014a), and the appearance of N1s peak indicates that N-doping has been realized (Liu et al. 2009; Shi et al. 2014a) [the peak of N1s has been analyzed in our

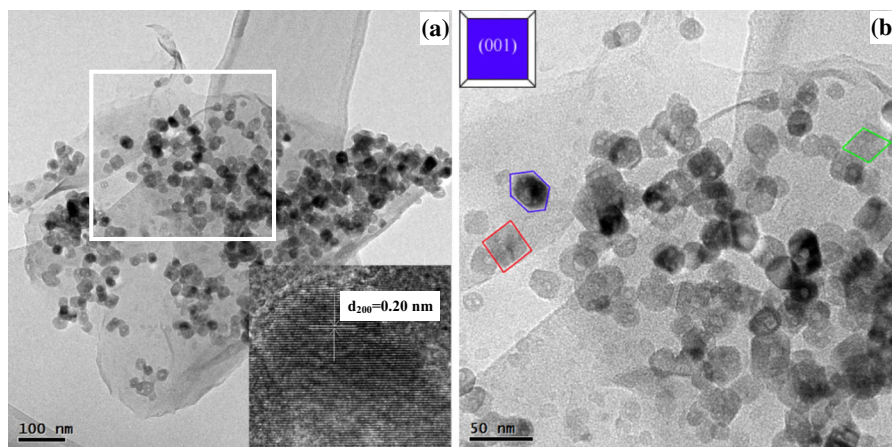


Fig. 2 TEM images of typical sample NTNP/GR-1.0 with low magnification (a) and high magnification (b). (Color figure online)

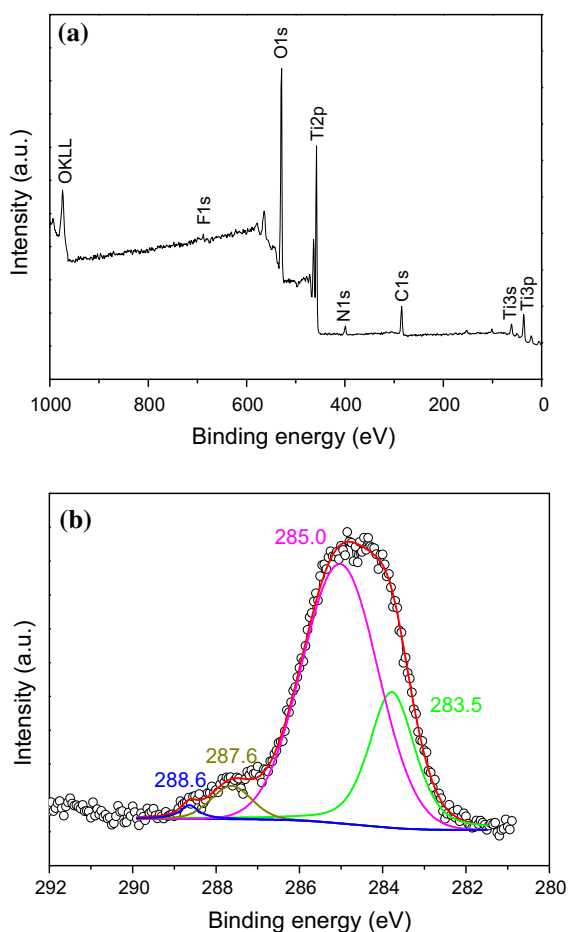


Fig. 3 a The XPS full survey of NTNP/GR-1.0; b the high-resolution C1s spectra of NTNP/GR-1.0. (Color figure online)

early work (Ai et al. 2014)]. Figure 3b displays the C1s high-resolution XPS spectrum of NTNP/GR-1.0. Four peaks at binding energies of 283.5, 285.0, 287.6, and 288.6 eV can be fitted, respectively. The peak at 285.0 eV can be attributed to the C–C, C=C, and C–H bonds (sp^2) of graphene. The peak located at 287.6 eV can be attributed to the oxygen-containing carbonaceous bonds (containing C–OH and C=O bonds) (Yumitori 2000; Chiang and Seitz 2001; Akhavan and Ghaderi 2009; Yang et al. 2009a), which depresses significantly in comparison with the C1s high-resolution XPS spectrum of GO (Fig. 5 in our previous work (Shi et al. 2014b)). The reason can be ascribed to the reduction of GO to GR due to the heat-treatment (Park and Ruoff 2009; Akhavan 2010). The peak at 283.5 eV is very close to the C1s peak of TiC (283.0 eV) (Park et al. 2006; Yin et al. 2007; Huang et al. 2008), which can be ascribed to the formation of O–Ti–C bonds by the substituting of carbon atoms to oxygen atoms in the lattice of TiO_2 (Park et al. 2006; Yin et al. 2007; Huang et al. 2008; Dong et al. 2009). The peak centered at 288.6 eV can be assigned to C–O bonds, which implies that Ti–O–C structure has formed via the replacing of carbon atoms to titanium atom in the lattice of TiO_2 (Gu et al. 2008; Wang et al. 2009). The Ti–O–C bonds formed in the interface between graphene and TiO_2 are similar to C-doping in TiO_2 lattices, which can arouse the red-shift of light absorption edge and the improvement of light absorption intensity.

Optical response property

The UV–vis diffuse reflectance spectra (DRS) of NTNP and NTNP/GR-1.0 are shown in Fig. 4. As confirmed in our previous publication (Ai et al. 2014), NTNP presents a light absorption platform in the region of 400–500 nm due to N-doping. Compared with NTNP, the NTNP/GR presents two prominent features: (i) the light absorption edge of NTNP/GR-1.0 shifts to longer wavelength, and (ii) the overall light absorption intensity is enhanced, which are highly consistent with the results deduced from the analysis of the high-resolution C1s. These features indicate that NTNP/GR can utilize the solar spectrum more efficiently in comparison with NTNP (Yu and Yu 2009).

Nitrogen adsorption–desorption analysis

The nitrogen adsorption–desorption and the corresponding pore-size distribution curves (inset in Fig. 5) of NTNP and NTNP/GR-1.0 are presented in Fig. 5. It can be observed that the two samples present similar isotherms with hysteresis loops, which implies the presence of mesopores in their structures. According to IUPAC classification, the hysteresis loops can be classified as type IV with type H3 (Kruk and Jaroniec 2001). Isotherms with type H3 loops have been ascribed to slitlike pores formed due to the aggregate of platelike particles (Kruk and Jaroniec 2001), which is in agreement with our results that nanoplates accumulate together (as revealed by TEM). The pore-size distributions demonstrate the existence of

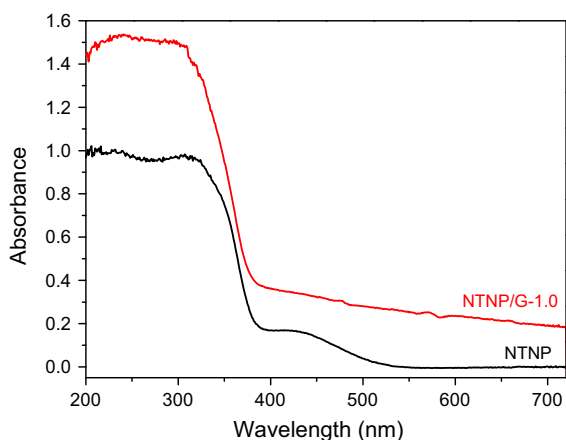


Fig. 4 UV–vis diffuse reflectance spectra of samples. (Color figure online)

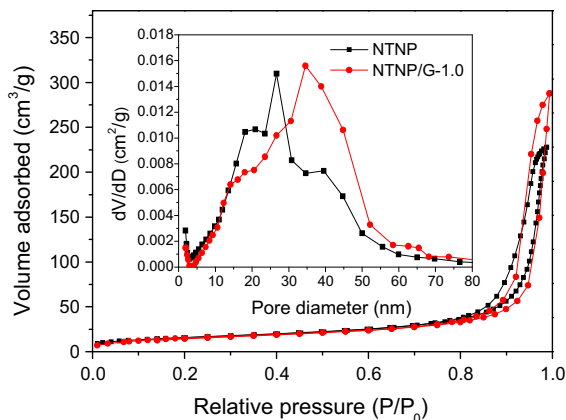


Fig. 5 Nitrogen adsorption–desorption isotherms and the pore-size distribution curves (inset) of NTNP and NTNP/GR-1.0. (Color figure online)

large numbers of mesopores. The specific surface area of the NTNP/GR-1.0 is $53.54 \text{ m}^2 \text{ g}^{-1}$, which is higher than that of NTNP ($51.50 \text{ m}^2 \text{ g}^{-1}$). The reason can be attributed to the introduction of graphene with an extremely high surface area ($2600 \text{ m}^2 \text{ g}^{-1}$ theoretical). It is well known that the high surface area is very helpful to the improvement of photocatalytic activity as sample with higher surface area can provide more possibility for the diffusion and transportation of target molecules and intermediates during the photocatalysis process.

Photoluminescence spectra

To study the charge anti-recombination effect resulted from of graphene, the photoluminescence (PL) spectra of NTNP and NTNP/GR-1.0 were carried out. As shown in Fig. 6, the PL spectrum of NTNP presents a strong emission peak at approximately 605 nm, and the peak intensity of NTNP/GR-1.0 is decreased obviously after the introduction of graphene, which indicates that the recombination of photo-excited electrons and holes has been restrained highly due to the excellent mobility of charge carriers resulted from graphene (Hou et al. 2013).

Photocatalytic activity

The photocatalytic decoloration of MB solution was used to evaluate the photocatalytic activities of all samples. For comparison, micrometer-sized N-doped TiO_2 plates with exposed {001} facets [NTP, the

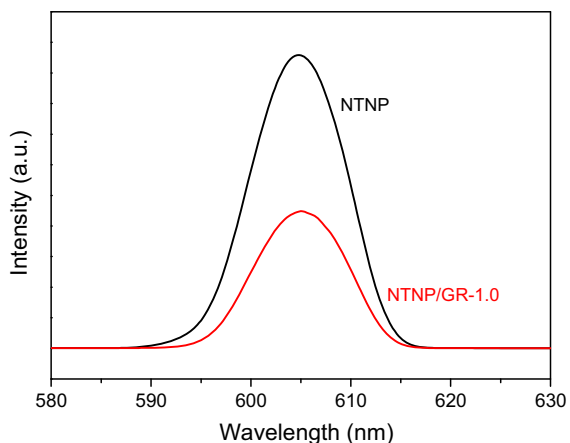


Fig. 6 Photoluminescence spectra of NTNP and NTNP/GR-1.0 excited at the wavelength of 300 nm. (Color figure online)

sample with the highest visible-light photocatalytic activity and labeled as S20 in our previous work (Shi et al. 2014a)] and the composite photocatalyst of NTP and graphene [NTP/GR, the sample with the highest visible-light photocatalytic activity and labeled as NTS/G-6 in our previous work (Shi et al. 2014b)] were also tested under the same conditions. Before photocatalysis, the solution including MB and catalyst was stirred in dark for 1 h to achieve the adsorption equilibrium. The results of the photocatalytic decoloration of MB solution under visible-light irradiation ($\lambda > 420$ nm) are displayed in Fig. 7. Due to the micrometer size and the low specific surface area, NTP presents the worst adsorption property among all samples, only 23 % of MB is removed from water in 1 h. Compared with NTP, the adsorption property

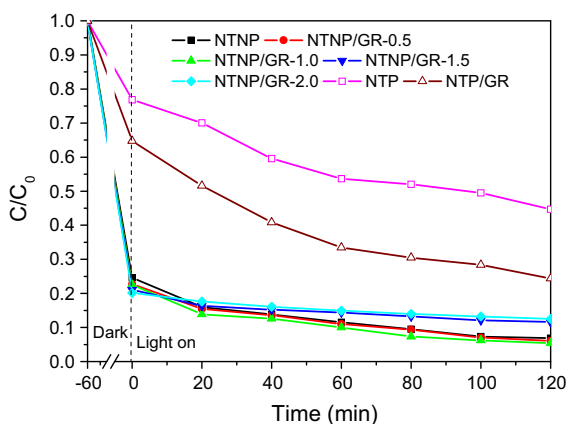


Fig. 7 Photocatalytic decoloration of MB solution over samples under visible light. (Color figure online)

NTP/GR is improved due to the introduction of graphene, and 35 % of MB is removed from water in 1 h. In contrast, NTNP and NTNP/GR samples present more excellent adsorption property, and more than 70 % of MB is removed from water in the same adsorption time (1 h). However, it is difficult to compare their photocatalytic activities due to the effect of strong adsorption.

In order to eliminate the effect of adsorption on the evaluation of photocatalytic activity, we designed a cyclic adsorption experiment to let these samples achieve adsorption saturation in dark. The cyclic adsorption experiment was performed as following steps (Shi et al. 2012a): first, 50 mg of samples was put in a 50-ml tube. Then, 50 ml of MB solution (10 mg l^{-1}) was transferred into the tube to begin the adsorption experiment. Throughout the adsorption experiment, the suspension was agitated continuously. 60 min later, 3 ml of suspension was removed out. After the solid particles in the suspension were eliminated by centrifugal separation, the filtrate was tested via a spectrophotometer to obtain the absorbance data. After one cycle was finished, 50 ml of MB solution (still 10 mg l^{-1}) was used to begin the next cycle. The adsorption experiment was repeated until the adsorption capacities of all samples disappeared completely. As shown in Fig. 8, the columnar value gradually enhances with the increasing cycle time for all the seven samples, indicating the adsorption capacities are disappearing gradually due to the absence of light irradiation. The columnar values are

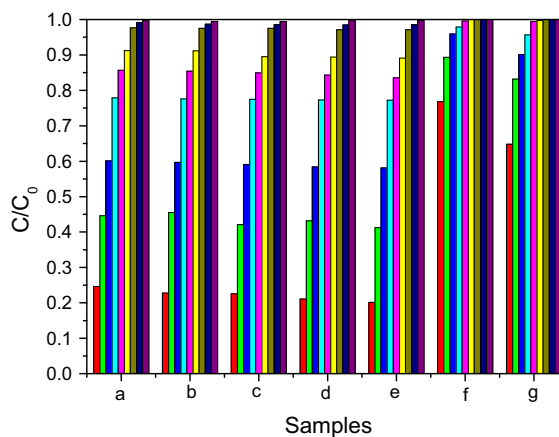


Fig. 8 Cyclic adsorption capacities of samples in dark for nine runs: a NTNP, b NTNP/GR-0.5, c NTNP/GR-1.0, d NTNP/GR-1.5, e NTNP/GR-2.0, f NTP, g NTP/GR. (Color figure online)

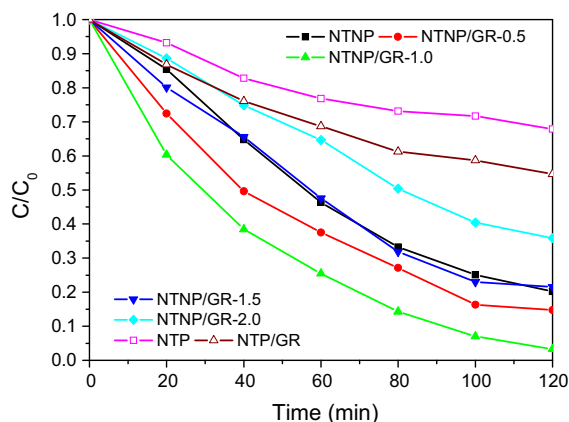


Fig. 9 Photocatalytic decoloration of MB solution over samples achieved adsorption saturation under visible light. (Color figure online)

almost close to the 1.0 at the ninth cycle, which implies that these samples have achieved adsorption saturation.

These samples achieved adsorption saturation were used as photocatalysts to decolorize MB solution under visible light ($\lambda > 420$ nm). As displayed in Fig. 9, NTP presents the worst photocatalytic activity among all samples due to its large particle size, low specific surface area, and the high recombination rate of photo-excited carriers. Due to the effective charge anti-recombination of graphene, NTP/GR presents higher photocatalytic activity than NTP. Compared with micrometer-sized NTP, the photocatalytic activity of NTNP is improved significantly due to its smaller particle size and higher specific surface area. Furthermore, the photocatalytic activity of composite photocatalysts (NTNP/GR-0.5 and NTNP/GR-1.0) is further enhanced owing to the charge anti-recombination effect of graphene. Due to the competition for light absorption between NTS and graphene, there is an optimal ratio between graphene and NTNP (1.0 % in present work) for the maximum of photocatalytic activity.

Proposed photocatalytic mechanism

Figure 10 schematically illustrates the photocatalytic mechanism of NTNP/GR under visible-light irradiation. Due to doping, a series of localized impurity states can be formed above valence band (VB) of TiO_2 . The electrons located in the localized impurity states can be excited to the conduction band (CB) of

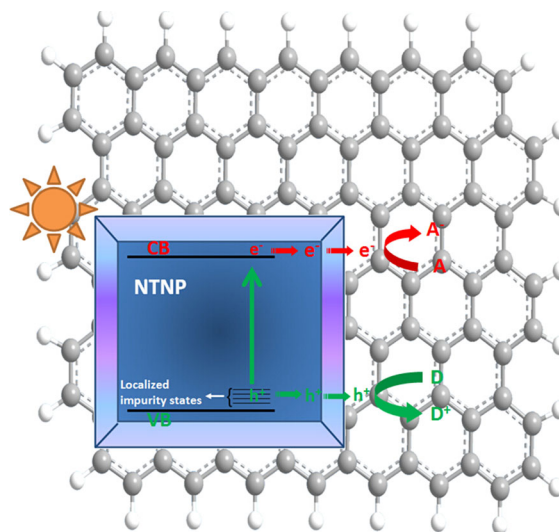
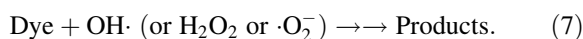
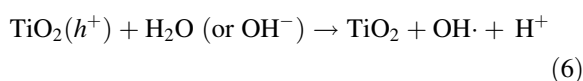
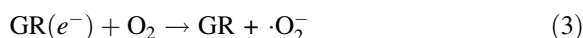
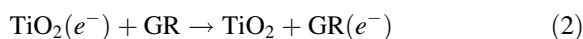
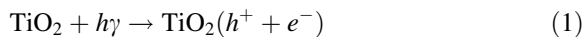


Fig. 10 Photocatalytic mechanism on the NTNP/GR under visible-light irradiation. (Color figure online)

TiO_2 under visible-light irradiation, and correspondingly left holes in the localized impurity states (Eq. 1). Due to the excellent mobility of charge carriers, these electrons can be transferred rapidly by graphene (Eq. 2). Subsequently, these electrons will be scavenged by molecular oxygen (aAcceptor) to produce the superoxide radical anion (Eq. 3) and hydrogen peroxide (Eq. 4). Then, these new radical groups interreact each other to yield hydroxyl radicals ($\text{OH}\cdot$) (Eq. 5). Meanwhile, the photo-excited holes in the localized impurity states can react with hydroxyl groups and water molecules (Donor) to yield $\text{OH}\cdot$ groups (Eq. 6). Finally, MB molecules will be oxidized by these oxidants step by step into final products (Eq. 7) (Fan et al. 2012; Shi et al. 2012b).



Conclusions

Nanocomposites consisted of graphene nanosheets, and nitrogen-doped anatase TiO₂ nanoplates with exposed {001} facets were successfully synthesized by a sol-gel process. Compared with micrometer-sized NTP and NTP/GR, the obtained nanocomposites presented much high photocatalytic activity for the decoloration of MB under visible light, which could be ascribed to three important factors: smaller particle size and higher specific surface area of NTNP, the charge anti-recombination effect of graphene, the red-shift of light absorption edge, and the enhanced light absorption intensity of nanocomposites.

Acknowledgments This work was sponsored by the National Natural Science Fund Committee–Baosteel Group Corporation Steel Joint Research Fund (U1460105), the Fundamental Research Funds for the Central Universities (1191320055), the Director Foundation of State Key Laboratory of Electrical Insulation and Power Equipment (EIPE14126), the Opening Project of State Key Laboratory of Inorganic Synthesis and Preparative Chemistry (2015-14), and the National Natural Science Foundation of China (51202294, 51201175). The valuable comments of anonymous reviewers are greatly appreciated.

References

- Ai HY, Shi JW, Duan RX, Chen JW, Cui HJ, Fu ML (2014) Sol-gel to prepare nitrogen doped TiO₂ nanocrystals with exposed 001 facets and high visible-light photocatalytic performance. *Int J Photoenergy*. doi:10.1155/2014/724910
- Akhavan O (2010) Graphene nanomesh by ZnO nanorod photocatalysts. *ACS Nano* 4:4174–4180. doi:10.1021/nn1007429
- Akhavan O, Ghaderi E (2009) Photocatalytic reduction of graphene oxide nanosheets on TiO₂ thin film for photoinactivation of bacteria in solar light irradiation. *J Phys Chem C* 113:20214–20220. doi:10.1021/jp906325q
- Allen MJ, Tung VC, Kaner RB (2010) Honeycomb carbon: a review of graphene. *Chem Rev* 110:132–145. doi:10.1021/cr900070d
- Asahi R, Morikawa T, Ohwaki T, Aoki K, Taga Y (2001) Visible-light photocatalysis in nitrogen-doped titanium oxides. *Science* 293:269–271. doi:10.1126/science.1061051
- Chen X, Mao SS (2007) Titanium dioxide nanomaterials: synthesis, properties, modifications, and applications. *Chem Rev* 107:2891–2959. doi:10.1021/cr0500535
- Chen JS, Tan YL, Li CM, Cheah YL, Luan D, Madhavi S, Chiang Boey FY, Archer LA, Lou XW (2010) Constructing hierarchical spheres from large ultrathin anatase TiO₂ nanosheets with nearly 100% exposed (001) facets for fast reversible lithium storage. *J Am Chem Soc* 132:6124–6130. doi:10.1021/ja100102y
- Chiang TC, Seitz F (2001) Photoemission spectroscopy in solids. *Ann Phys* 10:61–74. doi:10.1002/1521-3889(200102)10:1/2<61:AID-ANDP61>3.3.CO;2-7
- Diebold U (2003) The surface science of titanium dioxide. *Surf Sci Rep* 48:53–229. doi:10.1016/S0167-5729(02)00100-0
- Dong F, Wang H, Wu Z (2009) One-step “green” synthetic approach for mesoporous c-doped titanium dioxide with efficient visible light photocatalytic activity. *J Phys Chem C* 113:16717–16723. doi:10.1021/jp9049654
- Fan J, Liu S, Yu J (2012) Enhanced photovoltaic performance of dye-sensitized solar cells based on TiO₂ nanosheets/graphene composite films. *J Mater Chem* 22:17027–17036. doi:10.1039/c2jm33104g
- Fujishima A, Zhang X, Tryk DA (2008) TiO₂ photocatalysis and related surface phenomena. *Surf Sci Rep* 63:515–582. doi:10.1016/j.surfrep.2008.10.001
- Grabowska E, Diak M, Marchelek M, Zaleska A (2014) Decahedral TiO₂ with exposed facets: synthesis, properties, photoactivity and applications. *Appl Catal B* 156–157:213–235. doi:10.1016/j.apcatb.2014.03.019
- Gu DE, Lu Y, Yang BC, Hu YD (2008) Facile preparation of micro-mesoporous carbon-doped TiO₂ photocatalysts with anatase crystalline walls under template-free condition. *Chem Commun* 44:2453–2455. doi:10.1039/b800596f
- Han X, Kuang Q, Jin M, Xie Z, Zheng L (2009) Synthesis of titania nanosheets with a high percentage of exposed (001) facets and related photocatalytic properties. *J Am Chem Soc* 131:3152–3153. doi:10.1021/ja8092373
- Hoffmann MR, Martin ST, Choi W, Bahnemann DW (1995) Environmental applications of semiconductor photocatalysis. *Chem Rev* 95:69–96. doi:10.1021/cr00033a004
- Hou J, Yang C, Wang Z, Jiao S, Zhu H (2013) Bi₂O₃ quantum dots decorated anatase TiO₂ nanocrystals with exposed 001 facets on graphene sheets for enhanced visible-light photocatalytic performance. *Appl Catal B* 129:333–341. doi:10.1016/j.apcatb.2012.09.009
- Huang Y, Ho W, Lee S, Zhang L, Li G, Yu JC (2008) Effect of carbon doping on the mesoporous structure of nanocrystalline titanium dioxide and its solar-light-driven photocatalytic degradation of NO_x. *Langmuir* 24:3510–3516. doi:10.1021/la703333z
- Jing D, Jing L, Liu H, Yao S, Guo L (2013) Photocatalytic hydrogen production from refinery gas over a fluidized-bed reactor I: numerical simulation. *Ind Eng Chem Res* 52:1982–1991. doi:10.1021/ie3023127
- Khan SUM, Al-Shahry M, Ingler WB Jr (2002) Efficient photochemical water splitting by a chemically modified n-TiO₂. *Science* 297:2243–2245. doi:10.1126/science.1075035
- Kruk M, Jaroniec M (2001) Gas adsorption characterization of ordered organic-inorganic nanocomposite materials. *Chem Mater* 13:3169–3183. doi:10.1021/cm0101069
- Lee C, Wei X, Kysar JW, Hone J (2008) Measurement of the elastic properties and intrinsic strength of monolayer graphene. *Science* 321:385–388. doi:10.1126/science.1157996
- Li R, Zhang F, Wang D, Yang J, Li M, Zhu J, Zhou X, Han H, Li C (2013) Spatial separation of photogenerated electrons and holes among 010 and 110 crystal facets of BiVO₄. *Nat Commun* 4:2401–2407. doi:10.1038/ncomms2401

- Liu G, Yang HG, Wang X, Cheng L, Pan J, Lu GQ, Cheng HM (2009) Visible light responsive nitrogen doped anatase TiO₂ sheets with dominant 001 facets derived from TiN. *J Am Chem Soc* 131:12868–12869. doi:[10.1021/ja903463q](https://doi.org/10.1021/ja903463q)
- Liu G, Sun C, Smith SC, Wang L, Lu GQ, Cheng HM (2010a) Sulfur doped anatase TiO₂ single crystals with a high percentage of 001 facets. *J Colloid Interface Sci* 349:477–483. doi:[10.1016/j.jcis.2010.05.076](https://doi.org/10.1016/j.jcis.2010.05.076)
- Liu M, Piao L, Zhao L, Ju S, Yan Z, He T, Zhou C, Wang W (2010b) Anatase TiO₂ single crystals with exposed 001 and 110 facets: facile synthesis and enhanced photocatalysis. *Chem Commun* 46:1664–1666. doi:[10.1039/B924172H](https://doi.org/10.1039/B924172H)
- Park S, Ruoff RS (2009) Chemical methods for the production of graphenes. *Nat Nanotechnol* 4:217–224. doi:[10.1038/nnano.2009.58](https://doi.org/10.1038/nnano.2009.58)
- Park JH, Kim SW, Bard AJ (2006) Novel carbon-doped TiO₂ nanotube arrays with high aspect ratios for efficient solar water splitting. *Nano Lett* 6:24–28. doi:[10.1021/nl051807y](https://doi.org/10.1021/nl051807y)
- Shi JW, Cui HJ, Chen JW, Fu ML, Xu B, Luo HY, Ye ZL (2012a) TiO₂/activated carbon fibers photocatalyst: effects of coating procedures on the microstructure, adhesion property, and photocatalytic ability. *J Colloid Interface Sci* 388:201–208. doi:[10.1016/j.jcis.2012.08.038](https://doi.org/10.1016/j.jcis.2012.08.038)
- Shi JW, Cui HJ, Zong X, Chen S, Chen J, Xu B, Yang W, Wang L, Fu ML (2012b) Facile one-pot synthesis of Eu, N-codoped mesoporous titania microspheres with yolk-shell structure and high visible-light induced photocatalytic performance. *Appl Catal A* 435–436:86–92. doi:[10.1016/j.apcata.2012.05.044](https://doi.org/10.1016/j.apcata.2012.05.044)
- Shi JW, Zong X, Wu X, Cui HJ, Xu B, Wang L, Fu ML (2012c) Carbon-doped titania hollow spheres with tunable hierarchical macroporous channels and enhanced visible light-induced photocatalytic activity. *ChemCatChem* 4:488–491. doi:[10.1002/cctc.201200019](https://doi.org/10.1002/cctc.201200019)
- Shi JW, Ai HY, Chen JW, Cui HJ, Yang S, Li S, Fu ML (2014a) Nitrogen doped titania plates with dominant 001 facets: microstructure and property evolution, and their photocatalytic activities. *J Mol Catal A* 395:420–427. doi:[10.1016/j.molcata.2014.09.007](https://doi.org/10.1016/j.molcata.2014.09.007)
- Shi JW, Ai HY, Chen JW, Cui HJ, Fu ML (2014b) The composite of nitrogen-doped anatase titania plates with exposed 001 facets/graphene nanosheets for enhanced visible-light photocatalytic activity. *J Colloid Interface Sci* 430:100–107. doi:[10.1016/j.jcis.2014.05.027](https://doi.org/10.1016/j.jcis.2014.05.027)
- Sun W, Sun K, Peng T, You S, Liu H, Liang L, Guo S, Zhao XZ (2014) Constructing hierarchical fastener-like spheres from anatase TiO₂ nanosheets with exposed 001 facets for high-performance dye-sensitized solar cells. *J Power Sources* 262:86–92. doi:[10.1016/j.jpowsour.2014.03.086](https://doi.org/10.1016/j.jpowsour.2014.03.086)
- Wang HQ, Wu ZB, Liu Y (2009) A simple two-step template approach for preparing carbon-doped mesoporous TiO₂ hollow microspheres. *J Phys Chem C* 113:13317–13324. doi:[10.1021/jp9047693](https://doi.org/10.1021/jp9047693)
- Xiang QJ, Yu JG, Jaroniec M (2012) Graphene-based semiconductor photocatalysts. *Chem Soc Rev* 41:782–796. doi:[10.1039/C1CS15172J](https://doi.org/10.1039/C1CS15172J)
- Xu YJ, Zhuang YB, Fu XZ (2010) New insight for enhanced photocatalytic activity of TiO₂ by doping carbon nanotubes: a case study on degradation of benzene and methyl orange. *J Phys Chem C* 114:2669–2676. doi:[10.1021/jp909855p](https://doi.org/10.1021/jp909855p)
- Yang HG, Sun CH, Qiao SZ, Zou J, Liu G, Smith SC, Cheng HM, Lu GQ (2008) Anatase TiO₂ single crystals with a large percentage of reactive facets. *Nature* 453:638–641. doi:[10.1038/nature06964](https://doi.org/10.1038/nature06964)
- Yang D, Velamakanni A, Bozkolu G, Park S, Stoller M, Piner RD, Stankovich S, Jung I, Field DA, Ventrice CAJ, Ruoff RS (2009a) Chemical analysis of graphene oxide films after heat and chemical treatments by X-ray photoelectron and micro-Raman spectroscopy. *Carbon* 47:145–152. doi:[10.1016/j.carbon.2008.09.045](https://doi.org/10.1016/j.carbon.2008.09.045)
- Yang HG, Liu G, Qiao SZ, Sun CH, Jin YG, Smith SC, Zou J, Cheng HM, Lu GQ (2009b) Solvothermal synthesis and photoreactivity of anatase TiO₂ nanosheets with dominant 001 facets. *J Am Chem Soc* 131:4078–4083. doi:[10.1021/ja808790p](https://doi.org/10.1021/ja808790p)
- Yin S, Komatsu M, Zhang Q, Saito F, Sato TJ (2007) Improvement of thermal stability of nitrogen doped titania photocatalyst by addition of surfactants during solvothermal treatment. *J Mater Sci* 42:2240–2246. doi:[10.1007/s10853-007-2071-2](https://doi.org/10.1007/s10853-007-2071-2)
- Yu C, Yu JC (2009) A simple way to prepare C–N-codoped TiO₂ photocatalyst with visible-light activity. *Catal Lett* 129:462–470. doi:[10.1007/s10562-008-9824-7](https://doi.org/10.1007/s10562-008-9824-7)
- Yu A, Wu G, Zhang F, Yang Y, Guan N (2009) Synthesis and characterization of N-doped TiO₂ nanowires with visible light response. *Catal Lett* 129:507–512. doi:[10.1007/s10562-008-9832-7](https://doi.org/10.1007/s10562-008-9832-7)
- Yu J, Qi L, Jaroniec M (2010) Hydrogen production by photocatalytic water splitting over Pt/TiO₂ nanosheets with exposed (001) facets. *J Phys Chem C* 114:13118–13125. doi:[10.1021/jp104488b](https://doi.org/10.1021/jp104488b)
- Yumitori S (2000) Correlation of C1s chemical state intensities with the O-1s intensity in the XPS analysis of anodically oxidized glass-like carbon samples. *J Mater Sci* 35:139–146. doi:[10.1023/A:1004761103919](https://doi.org/10.1023/A:1004761103919)
- Zhang D, Li G, Yang X, Yu JC (2009) A micrometer-size TiO₂ single-crystal photocatalyst with remarkable 80% level of reactive facets. *Chem Commun* 45:4381–4383. doi:[10.1039/B907963G](https://doi.org/10.1039/B907963G)
- Zhang H, Lv X, Li Y, Wang Y, Li J (2010a) P25–graphene composite as a high performance photocatalyst. *ACS Nano* 4:380–386. doi:[10.1021/mn901221k](https://doi.org/10.1021/mn901221k)
- Zhang Y, Tang ZR, Fu X, Xu YJ (2010b) TiO₂–graphene nanocomposites for gas-phase photocatalytic degradation of volatile aromatic pollutant: is TiO₂–graphene truly different from other TiO₂–carbon composite materials? *ACS Nano* 4:7303–7314. doi:[10.1021/nn1024219](https://doi.org/10.1021/nn1024219)
- Zhang H, Wang Y, Liu P, Han Y, Yao X, Zou J, Cheng H, Zhao H (2011) Anatase TiO₂ crystal facet growth: mechanistic role of hydrofluoric acid and photoelectrocatalytic activity. *ACS Appl Mater Interfaces* 3:2472–2478. doi:[10.1021/am200363p](https://doi.org/10.1021/am200363p)
- Zhang N, Zhang YH, Xu YJ (2012) Recent progress on graphene-based photocatalysts: current status and future perspectives. *Nanoscale* 4:5792–5813. doi:[10.1039/C2NR31480K](https://doi.org/10.1039/C2NR31480K)